

Original article

Analysis of the Impact of Geometric Parameters on the Hydrodynamic Characteristics of Swept Oscillating Hydrofoils

CHEN Zhuo^a, SUN Guang^b, JIAO Bo^{a*}^a School of Naval Architecture and Port Engineering, Shandong Jiaotong University, China, 907546938@qq.com^b School of Naval Navigation and shipping, Shandong Jiaotong University, China, 13293334293@163.com^{a*} School of Naval Architecture and Port Engineering, Shandong Jiaotong University, China, W13293334293@126.com, Corresponding Author

Abstract

In the field of oscillating hydrofoil research, the choice of hydrofoils is still mainly based on traditional NACA airfoils. The article explores the hydrodynamic characteristics of other airfoil structures to further improve the applicable range of hydrofoil working environments. By applying the swept structure of fish tail fins through biomimetic methods to oscillating hydrofoils, a motion model of the swept oscillating hydrofoil is established, and the relevant mathematical expressions and parameter definitions are described. Through numerical simulation methods, the effects of the pitch axis position and the tip-to-root ratio on the performance of the swept oscillating hydrofoil are analyzed. The simulation results show that the pitch axis position has a significant impact on the various force characteristics and energy acquisition efficiency of the hydrofoil, while the tip-to-root ratio mainly reflects the degree of sweep of the hydrofoil, thereby affecting the lift-to-drag ratio and the moment coefficient of the swept hydrofoil. Selecting the appropriate pitch axis position and tip-to-root ratio will enhance the lift of the hydrofoil while reducing the drag experienced.

Keywords: Oscillating hydrofoil; Swept Wing; Numerical simulation; Mean Power Coefficient

1. Introduction

Energy is crucial for the survival and development of humanity. With environmental issues becoming increasingly severe, the gradual phasing out and replacement of fossil fuels represent the most significant scientific, technological, economic, and social challenge of the 21st century (ARMAROLI,2011). Among numerous clean and renewable energy sources, tidal energy has garnered widespread attention due to its unique advantages: compared to solar energy, tidal energy is more concentrated, with a density approximately 300 times that of solar energy(ZHANG,2021). In comparison to wind energy, tidal energy exhibits greater predictability and a density four times that of wind energy. When contrasted with wave energy, another form of marine energy, tidal energy stands out for its concentrated and stable energy supply, with fluctuations at only around 0.2% of wave energy. Globally, tidal energy reserves are estimated to be around 3000 GW, primarily concentrated in countries with extensive coastlines such as China, the United Kingdom, the United States, and Canada(SUN,CHEN,2024). Consequently, tidal energy has become a focal point of research and development, receiving significant support from various countries.

The oscillating hydrofoil power generation device is an emerging tidal energy conversion system in recent years. Due to the small aspect ratio of the hydrofoil, it can be deployed in shallow seas, shoals, and other areas. Therefore, compared to traditional rotating water turbines, it offers easy equipment maintenance, a lower initial investment, and its slow movement speed is more environmentally friendly to the local marine ecosystem (YOUNG,2012,2014,2017,2020) Since McKinney first proposed and experimentally verified the feasibility of energy capture by oscillating wings in 1981(KINSEY,2012,p.1), research on oscillating hydrofoils has been widely conducted. Pizal(1994) conducted experiments on wing shapes at different angles of attack, obtained instantaneous pressure data under air conditions, and examined the motion characteristics of three-dimensional wing shapes in cases of rotational stall, including average lift coefficient, drag coefficient, and pitching moment coefficient. Li(2012) performed numerical simulation analysis on the hydrodynamic characteristics of wings performing pitching motion in shear flow, studied the effect of

frequency on the mechanism of thrust of oscillating wings, and concluded that the propulsion efficiency is highest around a vibration frequency of 0.7. The Huang(2016,2017,2018) group analyzed and compared the oscillating force and work done of wings in heave and pitch motion using numerical simulation methods. The results indicate that the heave rate is proportional to the flapping frequency, and the Strouhal number is also proportional to the flapping frequency. Therefore, the difference in Strouhal numbers has a significant impact on the oscillating working force.

NACA airfoil profiles, characterized by their open data accessibility and low drag properties, are extensively used in theoretical studies of aircraft and hydrofoil wings. As research on oscillating hydrofoils progresses, scholars have endeavored to enhance the energy capture efficiency by improving traditional wing designs. Sun et al (2021). enhanced the NACA0018 hydrofoil by adding a movable trailing-edge Gurney flap. They investigated the impact of the Gurney flap at different lengths and motion frequencies on the energy capture efficiency of the hydrofoil under constant Reynolds numbers. Comparative analyses were conducted on the hydrodynamic coefficients between the hydrofoil with the trailing-edge Gurney flap, traditional hydrofoils, and hydrofoils with fixed Gurney flaps. The data suggested that combining the motion of the trailing-edge Gurney flap with oscillating hydrofoils contributes to improved energy capture efficiency.

Fish and Miklosovic(1978,1995,2006,2009,2011,2019) studied the underwater movement of humpback whales and discovered that the vortices generated by the distinctive tubercles along the leading edge of their pectoral fins help delay stall, increase lift, and reduce drag. They conducted wind tunnel experiments using an airfoil model with similar protrusions resembling the NACA 634-021 airfoil. Results indicated that the protrusions on the airfoil structure could increase maximum lift by over 6%, raise the critical stall angle by 40%, and reduce drag by up to 32%. This research directly demonstrates the feasibility of improving hydrofoil designs through biomimetic approaches.

Aquatic organisms such as fish exhibit a wide variety of body shapes and swimming techniques. Most fast and efficient fish utilize their caudal fins as the primary locomotor organs for activities such as acceleration,

steering, and rapid deceleration(Zhang,2012). Inspired by the work of the Fish team, this study applies a bio-inspired approach by incorporating the swept-back structure of fish caudal fins into an oscillating hydrofoil, analyzing its energy harvesting efficiency and relevant hydrodynamic characteristics.

2. Establishment of the Motion Model

2.1 Two-Dimensional hydrofoil Motion Model

Figure 1 depicts the parameter diagram of the oscillating hydrofoil. Here, LE is defined as the distance between the pitch axis center of the hydrofoil and the leading edge of the wing, TE represents the distance between the pitch axis center and the trailing edge of the wing, and c denotes the chord length of the hydrofoil, with the pitch axis center located along the chord length of the hydrofoil.

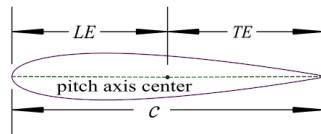


Fig. 1 Two-dimensional Oscillating Hydrofoil Geometric Model

The typical motion form commonly used for two-dimensional oscillating hydrofoils involves a combined pitching motion around the pitch axis center in a sinusoidal harmonic manner under the influence of the oncoming flow, along with a superimposed heaving motion in the vertical direction along the y -axis, as illustrated in Figure 2.

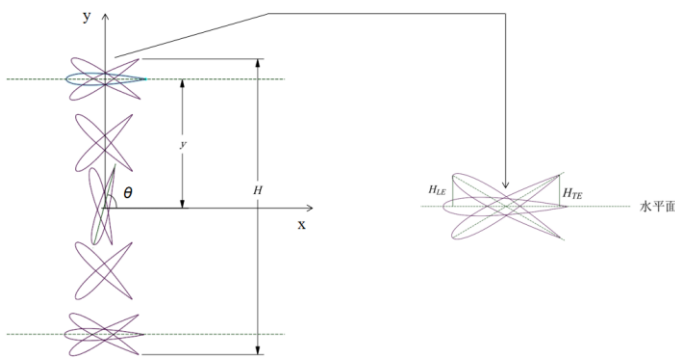


Fig. 2 Two-dimensional Oscillating Hydrofoil Motion Model

The conventional motion pattern commonly utilized for two-dimensional oscillating hydrofoils is as follows: where y represents the heave amplitude of the hydrofoil, H denotes the sweep height of the hydrofoil, and θ stands for the pitch angle of the hydrofoil. The sinusoidal motion equation for a conventional oscillating hydrofoil is expressed as:

$$y(t) = -y_p \sin(2\pi ft + \varphi) \quad (1)$$

$$\theta(t) = -\theta_p \sin(2\pi ft) \quad (2)$$

The conventional motion pattern widely employed for two-dimensional oscillating hydrofoils is as follows: where f represents the oscillation frequency, t denotes the current time, and φ stands for the heave-pitch phase angle (set to 90° in this study). When analyzing the situations where the hydrofoil reaches its top or bottom, as the pitching motion leads the heaving motion, both the leading and trailing edges of the hydrofoil will continue to oscillate at certain heights, denoted as H_{LE} and H_{TE} respectively. These heights vary with the movement of the pitch axis center of the hydrofoil and take the larger value.

Based on a summary from related literature including Sun(2012), the relationship between the sweep height of the hydrofoil, the heave amplitude, and the position of the pitch axis can be expressed as:

$$H = \max \begin{cases} -2y \sin(2\pi ft + \varphi) + 2TE \sin[-\theta \sin(2\pi ft)] \\ -2y \sin(2\pi ft + \varphi) - 2LE \sin[-\theta \sin(2\pi ft)] \end{cases} \quad (3)$$

The conventional motion form commonly utilized for two-dimensional oscillating hydrofoils aims to eliminate analytical difficulties arising from the unsteadiness and non-uniformity of the incoming flow field, leading to variations in flow velocity and differences in hydrofoil geometric parameters. To address these challenges, two significant dimensionless parameters, the Reynolds number Re_c and the reduced frequency f^* , have been introduced. Here, U_∞ represents the freestream velocity, and ν denotes the kinematic viscosity of the fluid:

$$Re_c = U_\infty c / \nu \quad (4)$$

$$f^* = fc / U_\infty \quad (5)$$

2.2 Motion Model of Trailing-Edge Oscillating Hydrofoil

In Figure 3, by keeping the trailing edge of the conventional hydrofoil unchanged and altering the ratio of chord lengths between the wingtips and the midsection (known as the taper ratio), we obtain a Trailing-Edge Oscillating Hydrofoil. Building upon the NACA0015 hydrofoil as a basis, this study defines the wingspan as A , the root chord as R , and the tip chord as T . Similar to conventional two-dimensional oscillating hydrofoils, the trailing-edge oscillating hydrofoil also

adheres to a sinusoidal motion pattern.

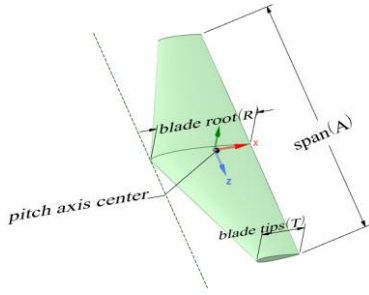


Fig. 3 Swept-type Oscillating Hydrofoil Structure

Due to the variation in the planform area, the formula for calculating the sweep height will change according to the taper ratio and the pitch axis location. Figure 4 illustrates the parameter conditions when the taper ratio is relatively small and the pitch axis is positioned near the trailing edge of the hydrofoil. When the hydrofoil reaches its peak position, due to the unique characteristics of the leading edge structure, it is necessary to separately calculate its sweep height and compare it with the trailing edge sweep height to determine the true sweep height of the hydrofoil for efficiency calculations.

Defining the distance between the pitch axis center and the leading edge of the wing root as L_R , and the distance to the leading edge of the wing tip as L_T , R_H as the sweep height at the leading edge of the root chord, and T_H as the sweep height at the leading edge of the tip chord. Due to the presence of the sweep angle, the part exceeding the wing tip when the hydrofoil reaches its peak forms a triangle. Therefore, its sweep height should be $(R_H+T_H)/2$. The actual swept area S_A of the triangle during the sweep process can be approximated as:

$$S_A = \frac{AR_H}{4} \quad (6)$$

Therefore, the actual sweep height of the hydrofoil is: $(R_H+T_H)/4$

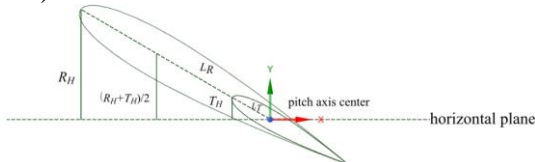


Fig. 4 Apex Sweep Height of the Hydrofoil

Based on the principle of triangle similarity,

$$T_H = \frac{L_T R_H}{L_R} \quad (7)$$

Therefore, equation (3) is revised as:

$$H = \max \begin{cases} -2y \sin(2\pi ft + \varphi) + 2TE \sin[-\theta \sin(2\pi ft)] \\ -2y \sin(2\pi ft + \varphi) - LE \frac{(L_T + L_R)}{L_R} \sin[-\theta \sin(2\pi ft)] \end{cases} \quad (8)$$

2.3 Calculation of Energy Efficiency for Trailing-Edge Oscillating Hydrofoils

In the study, since the incident flow represents the sole energy source captured by the hydrofoil, the focus lies on the influence of the incident flow while neglecting the internal forces acting on the hydrofoil system. As the flow passes over the hydrofoil, a resultant force $F(t)$, varying with the hydrofoil's motion state and perpendicular to the hydrofoil direction, is generated. This force is resolved into lift $L(t)$ perpendicular to the incident flow and drag $D(t)$ parallel to the incident flow. Simultaneously, the resultant force $F(t)$ exerts a moment $M(t)$ about the hydrofoil's axis of rotation. The dimensionless lift coefficient $C_L(t)$, drag coefficient $C_D(t)$, and moment coefficient $C_M(t)$ are defined.:

$$C_{L(t)} = L(t) / \frac{1}{2} \rho U_\infty^2 S \quad (9)$$

$$C_{D(t)} = D(t) / \frac{1}{2} \rho U_\infty^2 S \quad (10)$$

$$C_{M(t)} = M(t) / \frac{1}{2} \rho U_\infty^2 S c \quad (11)$$

In the equation, ρ represents the fluid density, U_∞ is the incident flow velocity, and S is the hydrofoil's frontal area. The instantaneous power P captured by the hydrofoil is the sum of the workdone by lift and the work done by the pitching moment:

$$P = L \cdot v + M \cdot \omega \quad (12)$$

The average power coefficient is:

$$\overline{C_P} = \overline{C_{PL}} + \overline{C_{PM}} = \frac{1}{T} \left[\int_0^T C_{PL} dt + \int_0^T C_{PM} dt \right] \quad (13)$$

Let S_0 be the swept area of the hydrofoil, and P_0 denote the total power captured by the oscillating hydrofoil:

$$P_0 = \frac{1}{2} \rho U_\infty^3 S_0 \quad (14)$$

From this, the energy capture efficiency η of the oscillating hydrofoil is:

$$\eta = \overline{P} / P_0 = \overline{C_P} \frac{c}{H} \quad (15)$$

3. Numerical simulation method and grid-independence verification

3.1 Verification of Simulation Methods

Based on the Fluent model, a hybrid approach combining dynamic mesh and sliding mesh models was employed to induce sinusoidal motion in an entirely active hydrofoil using User Defined Functions (UDF). Figure 5 illustrates the sliding mesh model, where the rectangular outflow domain has a width of $50c$, the circular fluid domain has a diameter of $3c$, with a total of 3×10^4 grid nodes and 500 nodes for the hydrofoil. The time step is set at 1×10^{-3} s.

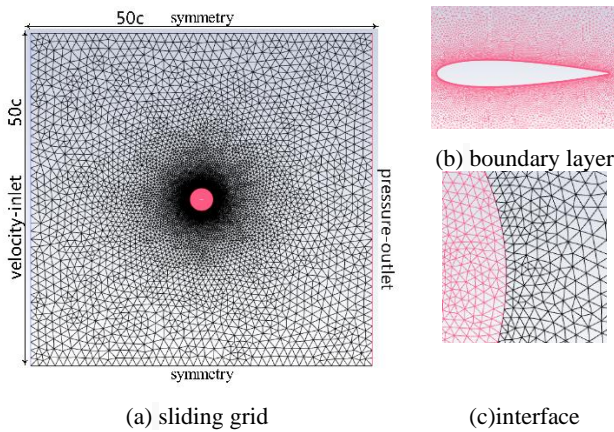


Fig. 5 Sliding Grid Model

To validate the correctness of the numerical simulation method and motion model, this study selects the relatively stable third cycle under the grid parameters and operating conditions, comparing it with the research conducted by Kinsey (KINSEY,2012,p.1). The results are presented in Table 1, where C_{Lmax} represents the maximum lift coefficient, while \bar{C}_D denotes the average drag coefficient, C_{Mmax} signifies the maximum pitch moment coefficient, and \bar{C}_P represents the average power coefficient. Through comparison, it is evident that the numerical simulation method employed in this study is reasonable.

Tab. 1 Comparison of Computational Results

Model	C_{Lmax}	\bar{C}_D	C_{Mmax}	\bar{C}_P
Kinsey	2.819	1.757	0.565	0.986
Artical	2.742	1.773	0.574	0.973

3.2 Grid Independence Verification

To mitigate the influence of grid density and time step on the computational results, a grid independence verification was conducted on the three-dimensional aft-

swept oscillating hydrofoil model in this study. The comparison results after employing four different grid quantities for the hydrofoil structure and flow field are presented in Table 2.

Tab. 2 Grid Independence Study Verification

Cells/ million	C_{Lmax}	\bar{C}_D	C_{Mmax}	\bar{C}_P
1.07	3.652	1.675	1.276	0.188
1.25	3.682	1.668	1.279	0.198
1.44	3.685	1.669	1.279	0.198
1.72	3.629	1.661	1.247	0.197

It can be observed that when the grid quantity ranges from 1.25×10^6 to 1.72×10^6 , the numerical values of the grid tend to stabilize. However, around 1.07×10^6 , there is still a 5.05% difference in the average power coefficient compared to the stable region. Therefore, the grid partitioning with a quantity of 1.44×10^6 is chosen as the grid model for the hydrofoil.

4. Research Results and Analysis

Understanding the influence of specific geometric parameters on hydrofoil performance, such as the tip root ratio and pitch axis position, can provide a theoretical basis for designing more efficient hydrofoils, enhancing flexibility and the range of choices during design. This study employs the S-A turbulence model with a Reynolds number of $Rec=5 \times 10^5$, an average chord length of $c=0.25$ m, an incoming flow area of $S=0.25$ m², a span of $A=1$ m, a reduced frequency of $f^*=0.14$, an amplitude of oscillation $y=c=0.25$ m, and a pitch amplitude of 75° . Under these conditions, the hydrodynamic performance effects of the pitch axis position and tip root ratio on a swept-back oscillating hydrofoil are examined.

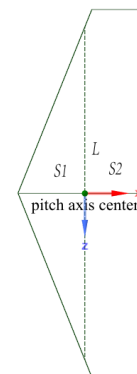


Fig. 6 Pitch Axis Location

Taking the pitch axis center as the origin, extend a line along the z-axis intersecting the edges of the hydrofoil.

The line obtained, denoted as L , is termed the pitch axis. When projecting the hydrofoil onto the XZ plane, as shown in Figure 6, the pitch axis L divides the shape into two areas: $S1$ near the leading edge and $S2$ near the trailing edge. Therefore, the pitch axis position can be determined by the value of $S1/(S1+S2)$. This value, representing the physical significance, is named as s . The study conditions and corresponding energy capture efficiency are detailed in Table 3.

Tab. 3 Working Condition Configuration

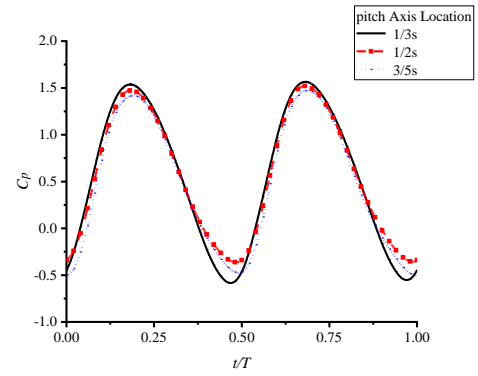
Tip Chord Length	Root Chord Length	Taper Ratio	Pitch Axis Location	$\eta(\%)$
		1/3	1/3s	20.96
0.125	0.375	1/3	1/2s	20.43
		1/3	3/5s	17.95
		3/7	1/3s	22.29
0.15	0.35	3/7	1/2s	22.97
		3/7	3/5s	18.38
		2/3	1/3s	22.66
0.2	0.3	2/3	1/2s	24.42
		2/3	3/5s	20

4.1 Influence of Pitch Axis Position on the Hydrodynamic Performance of Aft-Swept Hydrofoils

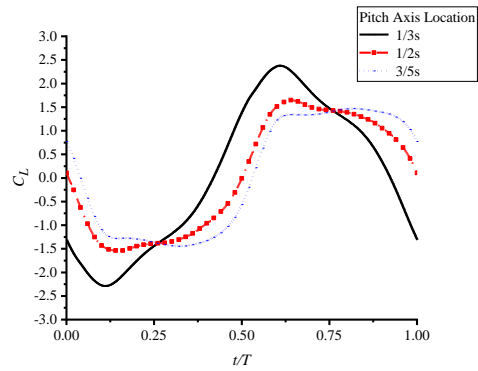
In Figure 7, under the condition of the most pronounced aspect ratio of 1/3, the curves of various hydrodynamic performance parameters for different pitch axis positions show that the pitch axis position of aft-swept hydrofoils has a relatively minor impact on the average power coefficient. Comparing the cases where the pitch axis is located at 1/2s and 3/5s, it is evident that for the 1/3s position, the lift coefficient exhibits a larger variation range between 1/8T to 3/8T and 5/8T to 7/8T, with the maximum lift coefficient exceeding that of the other two cases. However, the trends in drag coefficient are similar for all three cases, reaching maximum values around 1/4T and 3/4T.

It can be observed that as the pitch axis position gradually moves closer to the trailing edge, the lift decreases along with a reduction in drag for aft-swept hydrofoils. The moment variations are more distinct, with the moment coefficient at the 1/3s position exhibiting a significantly smaller magnitude of change compared to the other two cases, and reaching extreme

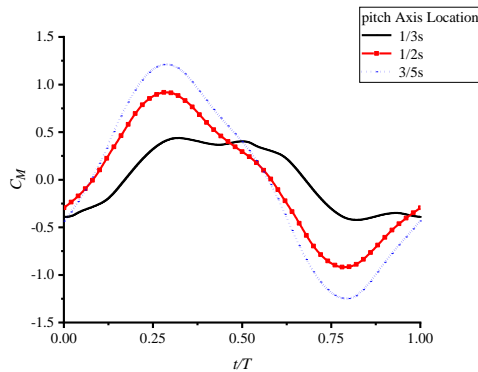
values around 1/4T and 3/4T.



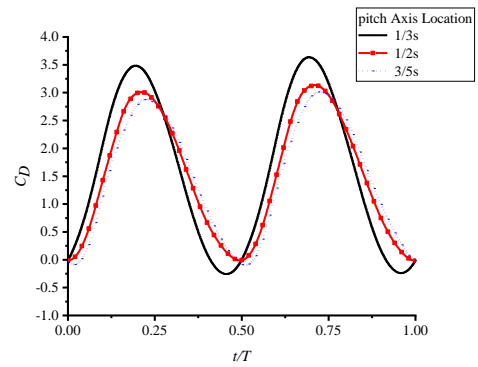
(a) power coefficient



(b) lift coefficient



(c) moment power coefficient



(d) drag coefficient

Figure 7: Parameters at Different Pitch Axis Locations for a 1/3 Taper Ratio

The cross-section of the aft-swept hydrofoil at the midsection, as shown in Figure 8, reveals significant

force differences at the $7/8T$ moment. By examining the pressure distribution at this moment, a more intuitive analysis can be made: when the pitch axis is positioned at $1/2s$ and $1/3s$, the lift on the lower surface of the hydrofoil is greater than that at the $1/3s$ position, but the area of negative pressure region on the upper surface is larger, resulting in higher drag.

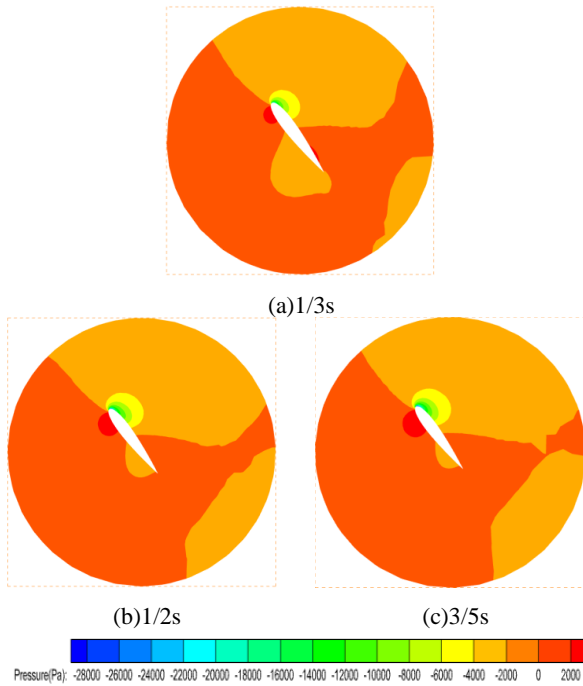


Figure 8 :Pressure Contour Maps at Different Pitch Axis Positions for a 1/3 Taper Ratio

At the same moment and with the same parameters, observing the vorticity plots of the five sections of the hydrofoil as shown in Figure 9, due to the aft-swept structure of the hydrofoil, the influence of the incoming flow on the midsection of the hydrofoil is significantly reduced compared to conventional straight wings. Instead, it is evenly distributed on both sides of the hydrofoil with variations in the sectional areas along the span.

In Figure 9(a), the vortices generated align closely with the hydrofoil, especially with lower vortex shedding intensity near the wingtip compared to Figure 9(b) and (c). Therefore, when the pitch axis is closer to the leading edge of the hydrofoil, the utilization of the incoming flow by the swept-wing hydrofoil is higher. However, at this moment, the lift coefficient of the hydrofoil is very small, so while vortex shedding may carry away some energy, the force distribution in the latter two cases better adheres to the energy capture principles of the hydrofoil.

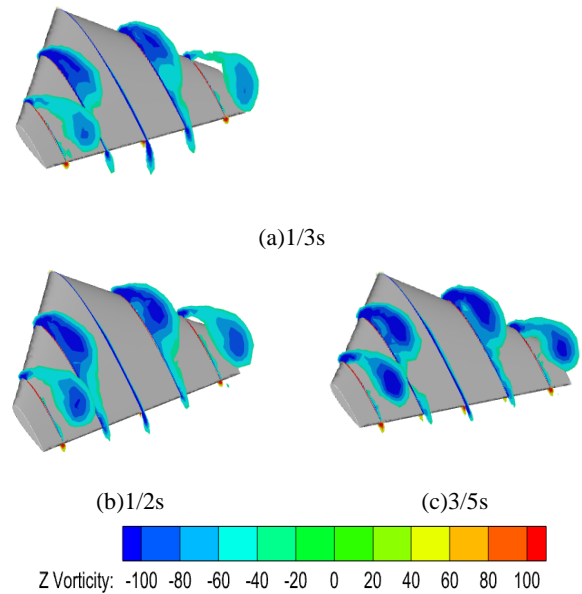
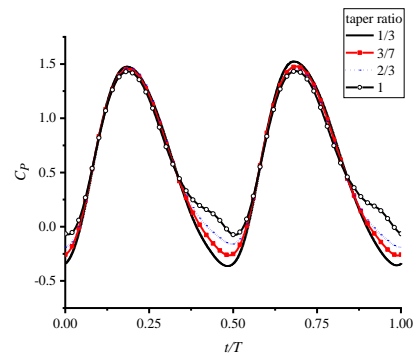


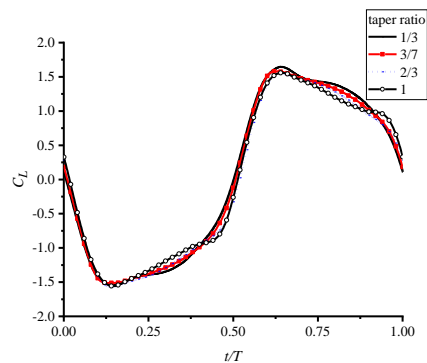
Figure 9 :Vorticity Contour Maps at Different Pitch Axis Positions for a 1/3 Taper Ratio

4.2 Influence of Aspect Ratio on the Hydrodynamic Performance of Aft-Swept Hydrofoils

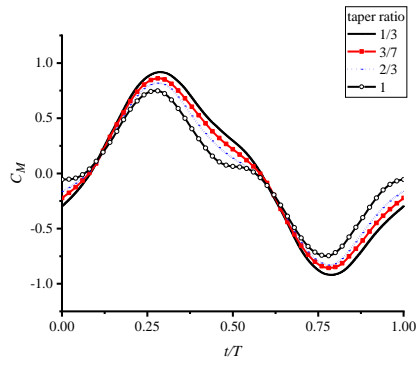
From Table 5, it is evident that the aft-swept hydrofoil achieves the highest energy capture efficiency when the pitch axis is located at $1/2s$. Therefore, based on this position, the hydrodynamic phenomena of aft-swept hydrofoils with aspect ratios of $1/3$, $3/7$, $2/3$, and a straight-wing hydrofoil with an aspect ratio of 1 are studied. The parameters for each case are depicted in Figure 10.



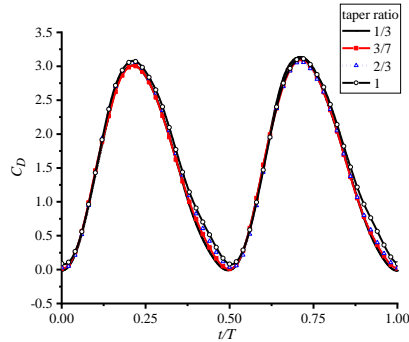
(a) power coefficient



(b) lift coefficient



(c) moment power coefficient



(d) drag coefficient

Figure 10 :Parameters for Different Semi-Span Ratios at the 1/2s Pitch Axis

Taking the average of the absolute values of the lift coefficient over one cycle yields a value known as \bar{C}_{LA} . Analyzing the lift and drag coefficients from Figure 10 yields Table 4.

Table 4 :Comparison of Lift-to-Drag Ratio for Different Semi-Span Ratios at the 1/2s Pitch Axis

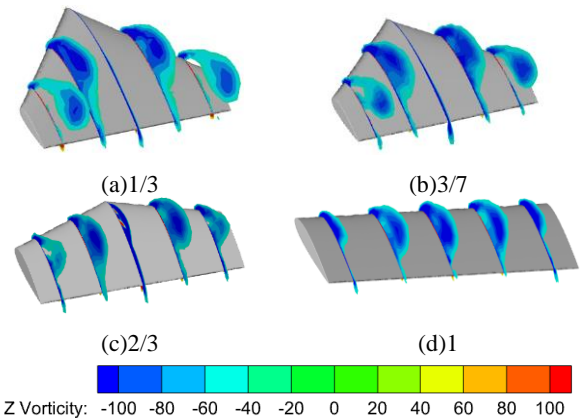
Taper Ratio	\bar{C}_{LA}	\bar{C}_D
1/3	1.127	1.511
3/7	1.108	1.515
2/3	1.087	1.535
1	1.090	1.594

From Figure 10, it can be observed that the effect of aspect ratio on the lift of the hydrofoil varies with the position in motion when the pitch axis is at 1/2s. Over half a cycle from 0.375T to 0.875T, the lift coefficient decreases with increasing aspect ratio, while over the other half of the cycle, it shows a positive correlation with the aspect ratio. The drag coefficient generally exhibits a trend where higher aspect ratios lead to higher drag coefficients. For larger aspect ratios, both the maximum and minimum drag coefficients of the hydrofoil are relatively higher.

Further analysis from Table 6 reveals that as the aspect ratio decreases, the hydrofoil exhibits higher lift coefficients and lower drag coefficients. With increasing

aspect ratio, the change in lift coefficient gradually slows down to almost constant, while the variation in drag coefficient increases.

The moment coefficient, where the influence of aspect ratio is more pronounced, aligns closer to the pressure center of high aspect ratios at this pitch axis position. From 1/4T to 1/2T and 3/4T to 1T, less negative work is done by the pitching moment, hence, although the maximum power coefficient is lower for higher aspect ratios compared to lower ones, the average power coefficient is higher due to the reduced negative work done by the pitching moment.

**Figure 11 :Vorticity Contour Maps for Different Taper Ratio at the 1/2s Pitch Axis**

Taking the example of the 7/8T moment, as shown in Figure 11, as the aspect ratio increases, the intensity of vortices passing through the hydrofoil gradually concentrates from the ends towards the center, showing a decreasing trend. In the case of a straight wing, there is minimal vortex shedding at the ends of the hydrofoil, and the vortex intensity distribution in the middle is relatively uniform.

Combining the pressure distribution on the upstream and downstream surfaces of the hydrofoil as shown in Figure 12, it can be observed that with smaller aspect ratios, the pressure on both surfaces becomes more concentrated. For instance, in Figure 12(a), at the tip and trailing edge of the hydrofoil, small high-pressure regions (>2000Pa) form, reducing the spanwise pressure distribution of the hydrofoil. In the case of the straight wing with the maximum aspect ratio, the pressure is essentially centered around the pitch axis, with the upstream and downstream surfaces of the hydrofoil exhibiting a complementary distribution. This is also why the hydrofoil does less work in terms of moments at this parameter setting.

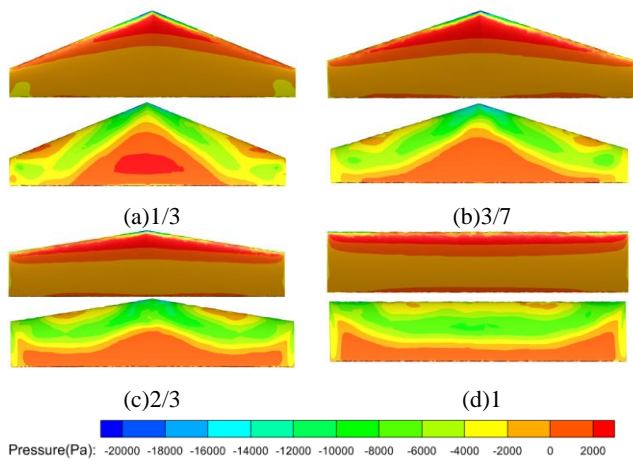


Figure 12 :Pressure Contour Maps for Different Taper Ratio at the 1/2s Pitch Axis

5. Conclusion

This passage discusses the effects of changing the chord length of the midsection and tip of a conventional hydrofoil to induce various degrees of sweep angle, and the impact of the pitch axis position and aspect ratio on the hydrodynamic performance of a swept-wing oscillating hydrofoil through numerical simulations. The conclusions drawn from this study are as follows:

(1) The pitch axis position of the swept-wing hydrofoil significantly influences its aerodynamic forces, contrary to traditional straight wings where peak power and efficiency are achieved near the leading edge. Due to the pressure center of the swept-wing hydrofoil being near the middle of the wing root, the pitch axis at this point, despite some energy dissipation from vortex shedding, still exhibits higher energy capture efficiency compared to the leading edge.

(2) Reducing the aspect ratio can increase the lift generated by the hydrofoil and decrease drag, with a more pronounced effect on lift enhancement as the aspect ratio decreases. The high lift and low drag characteristics of a low aspect ratio imply that the required lift can be obtained at lower flow speeds, reducing friction losses during hydrofoil motion and enhancing adaptability to varying sea conditions.

(3) The triangular structure at the leading edge of the swept-wing hydrofoil enhances its structural strength, disperses the impact of oncoming flow on the hydrofoil as a whole, and contributes to extending the hydrofoil's service life.

This study provides a theoretical basis for the design of swept-wing oscillating hydrofoils. Future research could focus on propulsion applications or further explore the

hydrodynamic performance of different structural types of hydrofoils, such as forward-swept and trapezoidal wings, as well as analyze different motion forms based on frequencies or pitch angles.

References

- ARMAROLI N, BALZANI V.(2011),Towards an electricity-powered world. *Energy and Environmental Science*, 4(9),pp.3193-3222.
- ZHANG J S, WANG G H, LIN X F.(2021), Overview of the Development and Utilization of Tidal Energy and Research on Key Scientific and Technological Issues.*Journal of Hohai University*, 49(03),pp. 220-232.
- SUN K, CHEN T Y.(2024) Current Status and Trends of Marine Current Energy Power Generation Technology Research.*Ship Engineering*,46(01), pp.16-27.
- YOUNG J, LAI J C S, PLATZER M F. (2014)A review of progress and challenges in flapping foil power generation. *Progress in Aerospace Sciences*, 67(2014),p p.1-28.
- ZHU Q. (2012),Energy harvesting by a purely passive flapping foil from shear flows. *Journal of Fluids and Structures*, 34(2012),pp.157-169.
- LIU Z Q, WANG Y Z, HUA X G.(2020),Numerical studies and proposal of design equations on cylindrical oscillating wave surge converters under regular waves using SPH. *Energy Conversion and Management*,203: 112242.
- ZHANG D, MA X, SI Y, et al. (2017), Effect of doubly fed induction GeneratorTidal current turbines on stability of a distribution grid under unbalanced voltage conditions. *Energies*,10(2): 212.
- KINSEY T, DUMAS G. (2012), Computational Fluid Dynamics Analysis of a Hydrokinetic Turbine Based on Oscillating Hydrofoils. *Journal of Fluids Engineering*, 134(2): 021104.
- PIZIALI R.(1994),2-D and 3-D oscillating wing aerodynamics for a range of angles of attack including stall.
- LI D Y, LIU N S, LU X Y, et al.(2012),Force characteristics and vortex shedding of a pitching foil in shear flows. *Journal of Hydrodynamics*, 17(1),pp.27-33.
- WANG Y, HUANG D G, HAN W, et al. (2017), Research on the mechanism of power extraction performance for flapping hydrofoils. *Ocean Engineering*.129,pp.626-636.
- WANG Y, SUN X J, HUANG D G, et al.(2016), Numerical investigation on energy extraction of flapping hydrofoils with different series foil shapes. *Energy*. 112,pp.1153-1168.
- SUN X J, ZHANG L C, HUANG D G, et al. (2018), New insights into aerodynamic characteristics of oscillating wings and performance as wind power generator. *International Journal of Energy Research*, 42(2),pp.776-789.
- SUN G, WANG Y, XIE Y D, et al. (2021), Research on the effect of a movable gurney flap on energy extraction of oscillating hydrofoil. *Energy*, 225: 120206.
- FRIEDLAENDER A S, HAZEN E L, NOWACEK D P, et al.(2009),Diel changes in humpback whale *Megaptera novaeangliae* feeding behavior in response to sand lance

Ammodytes spp. behavior and distribution. Marine Ecology Progress Series, 395,pp. 91-100.

HAZEN E L, FRIEDLAENDER A S, THOMPSON M A, et al.(2019),Fine-scale prey aggregations and foraging ecology of humpback whales *Megaptera novaeangliae*. Marine Ecology Progress Series, 395,pp. 75-89.

FISH F E, WEBER P W, MURRAY M M, et al.(2011), The Tubercles on Humpback Whales' Flippers: Application of Bio-Inspired Technology. Integrative and Comparative Biology, 51(1),pp.203-213.

EDEL R, WINN H.(1978),Observations on underwater locomotion and flipper movement of the humpback whale *Megaptera novaeangliae*. Marine Biology, 48,pp. 279-287.

FISH F E.(2006),The myth and reality of Gray's paradox: implication of dolphin drag reduction for technology. Bioinspiration and Biomimetics,1(2): R17.

FISH F E, BATTLE J M.(1995), Hydrodynamic design of the humpback whale flipper. Journal of Morphology, 225(1),pp.51-60.

ZHANG X.(2012),Hydrodynamic Research on Fish-like Tail Fin Propulsion System. Harbin: Harbin Engineering University.

SUN G.(2022),Research on the Hydrodynamic Characteristics of Flap-type Oscillating Hydrofoil Tidal Current Energy Generation Devices. Jinan: Shandong University.

Received 24 August 2024

1st Revised 14 November 2024

Accepted 23 December 2024